Molecular Crystals and Liquid Crystals Science and Technology. Section A. Molecular Crystals and Liquid Crystals
Publication details, including instructions for authors and subscription information:
http://www.tandfonline.com/loi/gmcl19

Organic Thin Films Studied by Surface Second-Harmonic Generation

Hideo Takezoe [a] , Kotaro Kajikawa [a] & Atsuo Fukuda [a]
[a] Department of Organic and Polymeric Materials, Tokyo Institute of Technology, O-okayama, Meguro-ku, Tokyo, 152, Japan
Version of record first published: 24 Sep 2006.

To cite this article: Hideo Takezoe , Kotaro Kajikawa & Atsuo Fukuda (1993): Organic Thin Films Studied by Surface Second-Harmonic Generation, Molecular Crystals and Liquid Crystals Science and Technology. Section A. Molecular Crystals and Liquid Crystals, 227:1, 93-112

To link to this article: http://dx.doi.org/10.1080/10587259308030964

Mol. Cryst. Liq. Cryst. 1993, Vol. 227, pp. 93–112
Reprints available directly from the publisher
Photocopying permitted by license only

Printed in the United States of America

ORGANIC THIN FILMS STUDIED BY SURFACE SECOND-HARMONIC GENERATION

HIDEO TAKEZOE, KOTARO KAJIKAWA
AND ATSUO FUKUDA
Department of Organic and Polymeric Materials,
Tokyo Institute of Technology, O-okayama, Meguro-ku,
Tokyo 152, Japan

Abstract After summarizing the problems in the quantitative analysis for structural and nonlinear optical quantities using surface second-harmonic generation, we review our experimental works on organic thin films. The samples are classified into two groups; vacuum evaporated films and Langmuir-Blodgett films. Based on the experimental results, we will point out the advantages of this method; (1) high sensitivity, (2) *in situ* observation and (3) spatial resolution.

INTRODUCTION

Organic thin films have been paid attention from the application point of view for functional devices. For the purpose, we have to construct well-organized structures, sometimes of molecular dimension. Then, we need a tool to assess the structure of monomolecular films. Among various techniques for studying organic thin films, surface second-harmonic generation (SHG) is one of the most sophisticated methods from many viewpoints.

Due to symmetry requirement, even-order nonlinear optical effect is not observable in centrosymmetric system. This fact brings about a main advantage that we can efficiently detect the signal from an interface or an ultra-thin film such as a monomolecular film on a centrosymmetric substrate. SHG also provides us with *in situ* observation of the dynamic structural change due to its coherent and high speed process.

After the pioneering works by Shen's group[1], surface SHG method has been applied to many types of films. In this article, we explain the method of analysis and point out matters which demand special attention. Then, we represent several experiments on vacuum evaporated films and LB films, showing the advantages of this method; (1) high sensitivity, (2) *in situ* observation and (3) spatial resolution.

ANALYSIS

Macroscopic and Microscopic Nonlinear Polarizabilities

SHG is one of the second-order nonlinear optical phenomena which arise from the second term of the following macroscopic polarization **P**;

$$\mathbf{P}=\chi^{(1)}:\mathbf{E}+\chi^{(2)}:\mathbf{EE}+\chi^{(3)}:\mathbf{EEE}+\cdots\cdots, \quad (1)$$

where $\chi^{(n)}$'s (n=2, 3, ·····) are n-th order nonlinear optical susceptibilities. In addition to the macroscopic nonlinear susceptibility, $\chi^{(n)}$, microscopic or molecular susceptibility is also a very important quantity from a viewpoint of molecular designing for nonlinear optics. Microscopic polarization **p** is written as

$$\mathbf{p}=\alpha:\mathbf{E}+\beta:\mathbf{EE}+\gamma:\mathbf{EEE}+\cdots\cdots, \quad (2)$$

where β and γ are second- and third-order nonlinear molecular susceptibilities, respectively. The summation of all **p** amounts to **P**. The relation between $\chi^{(2)}_{ijk}$ and $\beta_{\xi\eta\zeta}$ is given by

$$\chi^{(2)}_{ijk}=NL_i(2\omega)L_j(\omega)L_k(\omega)\langle\cos\Theta_{i\xi}\cos\Theta_{j\eta}\cos\Theta_{k\zeta}\rangle\beta_{\xi\eta\zeta}, \quad (3)$$

where N is a molecular density, $L_i(\Omega)$'s are local field factors at frequency Ω, $\Theta_{i\xi}$'s are angles between i and ξ axes and bracket stands for average over all molecules. Hereafter, we omit the superscript "(2)" of $\chi^{(2)}$ specifying second-order, if not necessary.

Procedure of Analysis

Let us first describe what we can obtain through surface SHG experiments. Since SH intensity is described by χ_{ijk} and polarizations of incident and SH light, we have to observe SH intensities using various combinations of polarizations to determine the ratio among all χ_{ijk}'s. Then we can determine the absolute χ_{ijk}'s by comparing with the data of standard sample such as quartz. The simplest way, though not quantitatively, to determine χ_{ijk}'s is the use of projection model[2]. In this model we consider only the projection of the incident and SH electric field, in other words, all the dielectric constants of a film and its surrounding are regarded as unity, so that no Fresnel reflection takes place.

With all χ_{ijk}'s on hand, we can determine an average molecular orientation Θ and $\beta_{\xi\eta\zeta}$ in some special cases under some assumptions. Here, we describe the procedure by taking an example of $C_{\infty v}$ symmetry with the symmetry axis along the film surface normal, z, which is most frequently seen in monomolecular films. The second-order nonlinear susceptibility tensor is given by

$$\chi^{(2)} = \begin{pmatrix} 0 & 0 & 0 & 0 & \chi_{xzx} & 0 \\ 0 & 0 & 0 & \chi_{yyz} & 0 & 0 \\ \chi_{zxx} & \chi_{zyy} & \chi_{zzz} & 0 & 0 & 0 \end{pmatrix}. \tag{4}$$

Because of the equivalence of x and y, $\chi_{zxx}=\chi_{zyy}$ and $\chi_{xzx}=\chi_{yzy}$. If we assume that there is only one predominant molecular susceptibility component, $\beta_{\xi\xi\xi}$, the nonzero components of χ_{ijk} are given by

$$\begin{aligned} \chi^s_{zzz} &= N_s L_z(2\omega) L_z^2(\omega) \langle \cos^3\Theta \rangle \beta_{\xi\xi\xi}, \\ \chi^s_{zxx} &= \chi^s_{zyy} = \frac{1}{2} N_s L_z(2\omega) L_x^2(\omega) \langle \cos\Theta \sin^2\Theta \rangle \beta_{\xi\xi\xi}, \\ \chi^s_{xzx} &= \chi^s_{yzy} = \frac{1}{2} N_s L_x(2\omega) L_z(\omega) L_x(\omega) \langle \cos\Theta \sin^2\Theta \rangle \beta_{\xi\xi\xi}, \end{aligned} \tag{5}$$

where suffix "s" stands for "surface", since we consider two-dimensional film; $\chi^s{}_{ijk}$ is a surface susceptibility and N_s is a

surface molecular density. If we make two assumptions; (1) the distribution of the polar angle of ξ axis with respect to z axis, Θ (see Fig.1), is given by the δ-function and the azimuth angle is randomly distributed and (2) anisotropy of L is neglected ($L_z(\omega)=L_i(\omega)$), we can determine the average molecular tilt angle from the surface normal, Θ, using the simple relation,

$$\tan^2\Theta = 2(\chi^s_{zxx}/\chi^s_{zzz}). \quad (6)$$

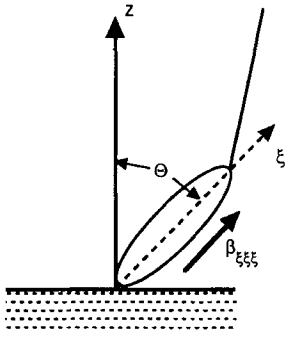

FIGURE 1 Orientation of uniaxial nonlinear chromophor with respect to surface normal.

In the projection model, it is enough to measure the p-polarized SH light generated by s- and p-polarized incident light, I^{sp} and I^{pp}, in order to determine χ_{zzz} and χ_{zxx}. If we further assume L=1, we can determine $\beta_{\xi\xi\xi}$. Thus, the surface SHG experiment provides us with microscopic as well as macroscopic nonlinear susceptibility in addition to the average molecular tilt angle, Θ. We should be careful, however, that there are several assumptions in the procedure. In the following, we will examine the assumptions used.

Quantitative Analysis

In order to analyze the surface SHG data more strictly, we have to take into account Fresnel reflection and its multiple reflection of the fundamental and SH light beams within a nonlinear active film. Hereafter, we omit the superscript "s" specifying "surface" in χ if not necessary. Based on the treatment by Bloembergen and

Pershan[3], the final forms of the reflected and transmitted SH light intensities, $I_1(2\omega)$ and $I_2(2\omega)$, are generally given by[4,5]

$$I_1(2\omega) = c_1\left(\left[\tilde{F}_{2,m,1}(2\omega)\,\hat{e}_1(2\omega)\right]\chi:\left[\tilde{F}_{2,m,1}(\omega)\hat{e}_1(\omega)\right]\left[\tilde{F}_{2,m,1}(\omega)\hat{e}_1(\omega)\right]\right)^2 I_1(\omega)^2,$$

$$I_2(2\omega) = c_2\left(\left[\tilde{G}_{2,m,1}(2\omega)\,\hat{e}_2(2\omega)\right]\chi:\left[\tilde{F}_{2,m,1}(\omega)\hat{e}_1(\omega)\right]\left[\tilde{F}_{2,m,1}(\omega)\hat{e}_1(\omega)\right]\right)^2 I_1(\omega)^2, \tag{7}$$

where

$$\tilde{F}_{i,j,k}(\Omega) = \tilde{G}_{k,j,i}(\Omega) = \begin{pmatrix} t^{xx}_{i,k}(\Omega) & 0 & 0 \\ 0 & t^{yy}_{i,k}(\Omega) & 0 \\ 0 & 0 & \left(\frac{\varepsilon_i(\Omega)}{\varepsilon_j(\Omega)}\right) t^{zz}_{i,k}(\Omega) \end{pmatrix}, \tag{8}$$

$$t^{xx}_{i,j}(\Omega) = \frac{2\sin\theta_j(\Omega)\cos\theta_j(\Omega)}{\sin(\theta_i(\Omega)+\theta_j(\Omega))\cos(\theta_j(\Omega)-\theta_i(\Omega))},$$

$$t^{yy}_{i,j}(\Omega) = \frac{2\sin\theta_j(\Omega)\cos\theta_i(\Omega)}{\sin(\theta_i(\Omega)+\theta_j(\Omega))}, \tag{9}$$

$$t^{zz}_{i,j}(\Omega) = \left(\frac{\sqrt{\varepsilon_i(\Omega)}}{\sqrt{\varepsilon_j(\Omega)}}\right)\frac{2\sin\theta_j(\Omega)\cos\theta_i(\Omega)}{\sin(\theta_i(\Omega)+\theta_j(\Omega))\cos(\theta_j(\Omega)-\theta_i(\Omega))},$$

$$c_h = \frac{32\pi^3\,\omega^2}{c^3\cos^2\theta_h(2\omega)\sqrt{\varepsilon_h(2\omega)}\,\varepsilon_h(\omega)}. \qquad (h=1,2) \tag{10}$$

The physical quantities used in the above equations are $\hat{e}_1(\omega)$: unit vector of an electric field of incident light, $\hat{e}_1(2\omega)$ and $\hat{e}_2(2\omega)$: those of SH light in the reflected and transmitted directions, $\theta_1(\omega)$: angle of incidence, $\theta_1(2\omega)$ and $\theta_2(2\omega)$: angles of reflection and refraction, respectively, $\varepsilon_1(\Omega)$ and $\varepsilon_2(\Omega)$: dielectric constants of media in the incident and transmitted sides at Ω, respectively.

Finally, in $C_{\infty v}$ symmetry, we obtain reflected SH intensities with incident and SH light polarization angles, γ_p and γ_a; $I(\gamma_p, \gamma_a)$, where the angle is defined as a rotation angle from the incident plane, as shown in Fig.2.

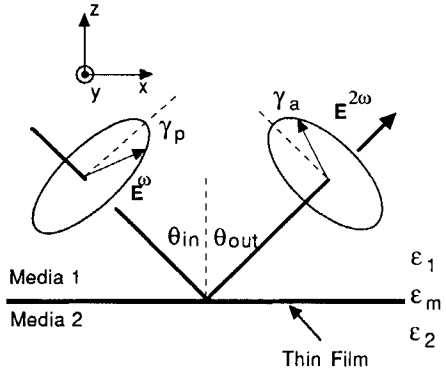

FIGURE 2 Optical geometry for the reflected SHG observation.

$$I(\gamma_p, 0°) = K\left(\cos^2\gamma_p\,(A\,\chi_{zzz} - B\,\chi_{xzx}) + \left(C\cos^2\gamma_p + D\sin^2\gamma_p\right)\chi_{zxx}\right)^2 I_1(\omega)^2, \tag{11}$$

$$I(\gamma_p, 90°) = K\left(E\sin\gamma_p\cos\gamma_p\,\chi_{yzy}\right)^2 I_1(\omega)^2, \tag{12}$$

$$I(\gamma_p, \gamma_p) = K\left[A\cos^3\gamma_p\,\chi_{zzz} + \left(C\cos^3\gamma_p + D\cos\gamma_p\sin^2\gamma_p\right)\chi_{zxx} + \left(-B\cos^3\gamma_p + E\cos\gamma_p\sin^2\gamma_p\right)\chi_{xzx}\right]^2 I_1(\omega)^2, \tag{13}$$

$$I(\gamma_p, \gamma_p{+}90°) = K\left[\cos^2\gamma_p\sin\gamma_p\,(A\,\chi_{zzz} - (E{+}B)\,\chi_{xzx}) + \left(C\cos^2\gamma_p\sin\gamma_p + D\sin^3\gamma_p\right)\chi_{zxx}\right]^2 I_1(\omega)^2, \tag{14}$$

where parameters A~E and K are given in Table I. The first two equations are p- and s-polarized SH intensities as a function of incident polarization angle, γ_p. The other equations are SH intensities as rotating the parallel and crossed polarizers, respectively. The simulated results have already been given in our previous paper[6].

Table I List of parameters used in eqs.(11)~(14).

$$A = 8\frac{\varepsilon_1(\omega)\varepsilon_2(\omega)\sqrt{\varepsilon_1(2\omega)}\sqrt{\varepsilon_2(2\omega)}}{\varepsilon_m(2\omega)\varepsilon_m^2(\omega)} \times \frac{\cos^2\theta_1(\omega)\sin^2\theta_1(\omega)\sin^2\theta_2(\omega)\sin^2\theta_1(2\omega)\sin\theta_2(2\omega)}{\cos^2(\theta_1(\omega)-\theta_2(\omega))\cos(\theta_1(2\omega)-\theta_2(2\omega))\sin^2(\theta_1(\omega)+\theta_2(\omega))\sin(\theta_1(2\omega)+\theta_2(2\omega))}$$

$$B = 16\frac{\sqrt{\varepsilon_1(\omega)}\sqrt{\varepsilon_2(\omega)}}{\varepsilon_m(\omega)} \times \frac{\cos^2\theta_1(\omega)\cos\theta_2(\omega)\cos\theta_1(2\omega)\cos\theta_2(2\omega)\sin\theta_1(\omega)\sin^2\theta_2(\omega)\sin\theta_2(2\omega)}{\cos^2(\theta_1(\omega)-\theta_2(\omega))\cos(\theta_1(2\omega)-\theta_2(2\omega))\sin^2(\theta_1(\omega)+\theta_2(\omega))\sin(\theta_1(2\omega)+\theta_2(2\omega))}$$

$$C = 8\frac{\sqrt{\varepsilon_1(2\omega)}\sqrt{\varepsilon_2(2\omega)}}{\varepsilon_m(2\omega)} \times \frac{\cos^2\theta_1(\omega)\cos^2\theta_2(\omega)\sin^2\theta_2(\omega)\sin^2\theta_1(2\omega)\sin\theta_2(2\omega)}{\cos^2(\theta_1(\omega)-\theta_2(\omega))\cos(\theta_1(2\omega)-\theta_2(2\omega))\sin^2(\theta_1(\omega)+\theta_2(\omega))\sin(\theta_1(2\omega)+\theta_2(2\omega))}$$

$$D = 8\frac{\sqrt{\varepsilon_1(2\omega)}\sqrt{\varepsilon_2(2\omega)}}{\varepsilon_m(2\omega)} \frac{\cos^2\theta_1(\omega)\sin^2\theta_2(\omega)\sin^2\theta_1(2\omega)\sin\theta_2(2\omega)}{\cos(\theta_1(2\omega)-\theta_2(2\omega))\sin^2(\theta_1(\omega)+\theta_2(\omega))\sin(\theta_1(2\omega)+\theta_2(2\omega))}$$

$$E = 16\frac{\sqrt{\varepsilon_1(\omega)}\sqrt{\varepsilon_2(\omega)}}{\varepsilon_m(\omega)} \frac{\cos^2\theta_1(\omega)\cos\theta_1(2\omega)\sin\theta_1(\omega)\sin^2\theta_2(\omega)\sin\theta_2(2\omega)}{\cos(\theta_1(\omega)-\theta_2(\omega))\sin^2(\theta_1(\omega)+\theta_2(\omega))\sin(\theta_1(2\omega)+\theta_2(2\omega))}$$

$$K = \frac{32\pi^3\omega^2 s c c^2\theta_1(2\omega)}{c^3\varepsilon_1(\omega)\sqrt{\varepsilon_1(2\omega)}}$$

The quantitative analysis was carried out by fitting the experimental results with the theoretical ones. The necessity of this procedure is clear from the fact that there exist different curves which have the same values for I(0°, 0°) (I^{pp}) and I(90°, 0°) (I^{sp}). These two curves result in the same χ_{zzz}/χ_{zxx}, if we only measure I^{pp} and I^{sp} for the analysis. Moreover, neglecting Fresnel reflection seriously influences the quantitative values of the parameters determined as will be discussed later. Thus, reliable analysis is only possible by such quantitative analysis.

Effect of Fresnel Reflection

Figure 3 shows the simulated results by the quantitative analysis and the projection model; I^{pp}/I^{sp} for 45° incidence is plotted against Θ in (a) reflection and (b) transmission geometries. It is clear that a certain I^{pp}/I^{sp} value gives different Θ values in these

two treatments. Thus, the projection model is less reliable from the quantitative viewpoint.

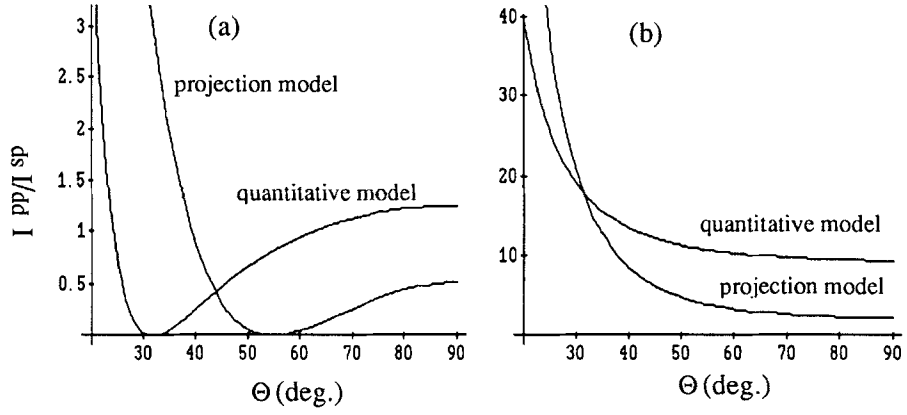

FIGURE 3 Simulated results for the quantitative analysis and the projection model; I^{pp}/I^{sp} is plotted against Θ in (a) reflection and (b) transmission geometries. The parameters used are $\varepsilon_2(\omega)=2.02$, $\varepsilon_2(2\omega)=2.10$, $\varepsilon_m(\omega)=2.25$ and $\varepsilon_m(2\omega)=2.72$.

Difference of SH Intensities in Different Optical Geometries

Let us take four optical geometries as depicted in Fig.4, where the incident beam is cast upon the film or substrate surface at 45° incidence. The projection model gives no difference in these SH intensities; $I_1 = I_3$ and $I_2 = I_4$ for I^{pp} and $I_1 = I_2 = I_3 = I_4$ for I^{sp}.

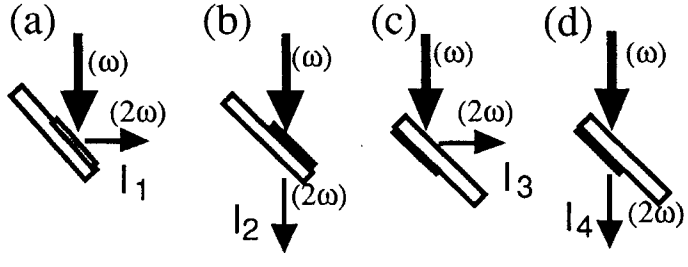

FIGURE 4 Optical geometries used.

Experimentally, however, three-times difference was observed especially in I^{sp} for a hemicyanine LB film[7]. The comparison between the experimental and simulated results using the quantitative analysis is shown in Fig.5. The agreement is satisfactory.

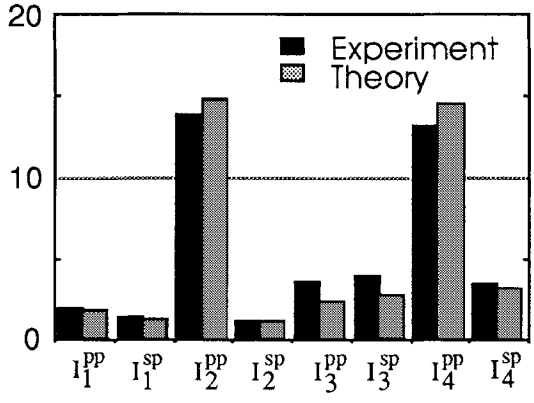

FIGURE 5 Comparison of the experimental and theoretical SH intensities.

Molecular Orientational Distribution

Even if we take the quantitative analysis, we have to assume the molecular orientational distribution function to calculate the average in eq.(5). Due to the easiness of treatment, we usually use the δ-function and simply eliminate the bracket. In order to assess the influence of the widening of the molecular orientational distribution, we simulate the relation between χ_{zzz}/χ_{zxx} and Θ. Equations (5) are rewritten as

$$\chi_{zzz} = N_s L_z(2\omega) L_z^2(\omega) \left(\frac{\int_0^{\frac{\pi}{2}} \cos^3\Theta \cdot g(\Theta, \sigma(\Theta), \Theta_0)\, d\Theta}{\int_0^{\frac{\pi}{2}} g(\Theta, \sigma(\Theta), \Theta_0)\, d\Theta} \right) \beta_{\xi\xi\xi}, \quad (15)$$

and etc., where

$$g(\Theta, \sigma(\Theta), \Theta_0) = \frac{1}{\sqrt{2\pi\sigma(\Theta)}} \exp\left(-\frac{(\Theta - \Theta_0)^2}{2\sigma(\Theta)}\right), \quad (16)$$

and Θ_0 is the center of the angular distribution and $\sigma(\Theta)$ is a standard deviation. By neglecting the local field factors, we obtain the results shown in Fig.6, where $\sigma(\Theta)=0$ corresponds to the δ-function. Quite reasonably, the dependence of χ_{zzz}/χ_{zxx} on Θ becomes small with increasing $\sigma(\Theta)$. Except for small Θ below 35°, the same χ_{zzz}/χ_{zxx} value gives somewhat larger Θ for larger $\sigma(\Theta)$.

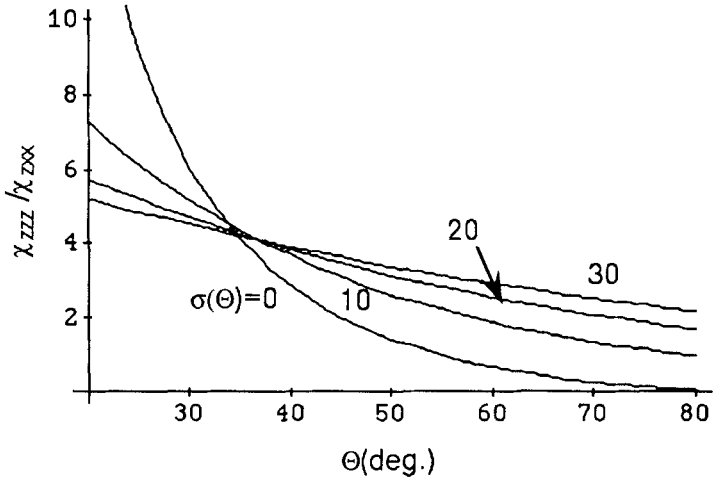

FIGURE 6 Effect of molecular orientational distribution on the analysis. Dependence of χ_{zzz}/χ_{zxx} on Θ for four $\sigma(\Theta)$'s.

Analysis of Films with In-Plane Anisotropy

Organic thin films sometimes have C_{2v} or C_s symmetry with in-plane anisotropy, which is formed, for instance, by flow alignment in LB film deposition or by in-plane field application in vacuum evaporation. We can use the same expression, eq.(7) for SH intensities. As for C_{2v} symmetry, the C_2 axis (z axis) is taken along the surface and then the tensor $\chi^{(2)}$ is also the same as eq.(4) except for the equivalence of x and y. Because of the in-plane anisotropy, it is convenient to simulate the SH intensities as a function of rotation angle of the film around the film surface normal to determine χ_{ijk}'s.

Surface Susceptibility and Bulk Susceptibility

If we have no standard surface whose surface susceptibility is known, we experimentally determine the surface susceptibility of monomolecular films or interfaces according to the equation

$$\chi^s(\text{film})=\frac{2}{\pi}\chi(\text{quartz})l_{coh}\left(\frac{I(\text{film})}{I(\text{quartz})}\right)^{1/2}\left(\frac{\varepsilon_m(\omega)\varepsilon_m(2\omega)^{1/2}}{\varepsilon_q(\omega)\varepsilon_q(2\omega)^{1/2}}\right), \quad (17)$$

where l_{coh} is the coherent length of quartz. Here the SH intensity should be measured in the transmission geometry, since the measurement of the bulk sample of quartz is made in this geometry. If we want to estimate the bulk susceptibility $\chi(\text{film})$ of the accumulated films from $\chi^s(\text{film})$, we need to have the thickness of the film, d, and to use the equation

$$\chi^s(\text{film})=d\chi(\text{film}). \quad (18)$$

The estimation of d is another problem in thin films such as a monomolecular layer. The bulk susceptibility is, however, important anyway only in bulk materials for practical use of submicron in thickness. For such films thicker than monomolecular thickness but enough thinner than the coherent length of the film, we directly obtain bulk susceptibility $\chi(\text{film})$ according to the equation

$$\chi(\text{film})=\frac{2}{\pi}\chi(\text{quartz})\left(\frac{l_{coh}}{d}\right)\left(\frac{I(\text{film})}{I(\text{quartz})}\right)^{1/2}\left(\frac{\varepsilon_m(\omega)\varepsilon_m(2\omega)^{1/2}}{\varepsilon_q(\omega)\varepsilon_q(2\omega)^{1/2}}\right). \quad (19)$$

using the film thickness d.

Much importance in the surface SHG experiment is to estimate the molecular susceptibility. In this sense, we obtain fairly reliable value in case of monomolecular film at the air/water interface, since we can accurately estimate the surface number density, N_s. Difficulty exists in estimating the local field factors. Only way to estimate the local field factors is to use L=1 together with the experimental data obtained at very large molecular area. An example will be shown later.

EXPERIMENTAL APPARATUS

We performed SHG experiments for monomolecular films at the air/water interface and on a substrate. The fundamental beam of Q-switched Nd:YAG laser (Quanta-Ray DCR 11) was cast upon the film surface with an incident angle of either 0° or 45° after reducing the light intensity less than 1 mJ per pulse using ND filters. The beam spot size was usually about 300 μm and sometimes properly chosen to be much smaller. The rotation of sample and polarizers was automatized using pulse motors and their drivers.

EXPERIMENTAL RESULTS

Polyurea

Poled polymers are one of the most promising second-order nonlinear optical materials mainly because of their good processability. Among them, polyurea is very unique, because of

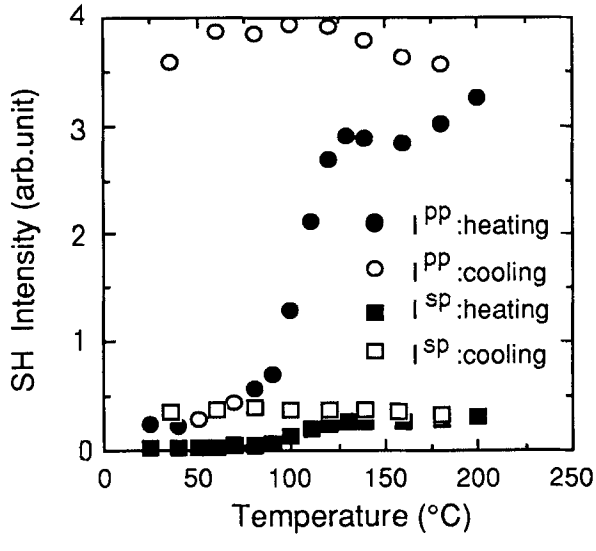

FIGURE 7 *In situ* observation of the temperature dependent SH intensities I_{pp} and I_{sp} under a corona discharging field in the heating and cooling processes.

the unprecedented thermal stability up to 200°C[8]. The film of the oligomer is prepared by vapor deposition polymerization from aromatic diamine and aromatic diisocyanate[9,10]. The stable poled structure is brought about by polymerization and crystallization progressing simultaneously with an electric-field-induced alignment[8].

We made *in situ* observation of the SH intensity change in the heating and cooling processes under a poling field by corona discharge[8]. The results, I^{pp} and I^{sp}, are shown in Fig.7. It is clear that a marked increase in the SH intensity is observed at 100~120°C. According to the fact that an efficient poling cannot be made once the film is heated without a poling field, importance of the simultaneous progress of the poling, polymerization and crystallization are obvious.

Poly(vinylidene fluoride)

Vapor deposition of polar organic materials in the presence of an electric field is expected to provide us with a very stable poled structure. We found that vapor deposited poly(vinylidene fluoride) (PVDF) films under an electric field along the substrate plate (z axis) show a stable poled structure[11]. Figure 8 shows examples of the SH intensity profiles for the films prepared under

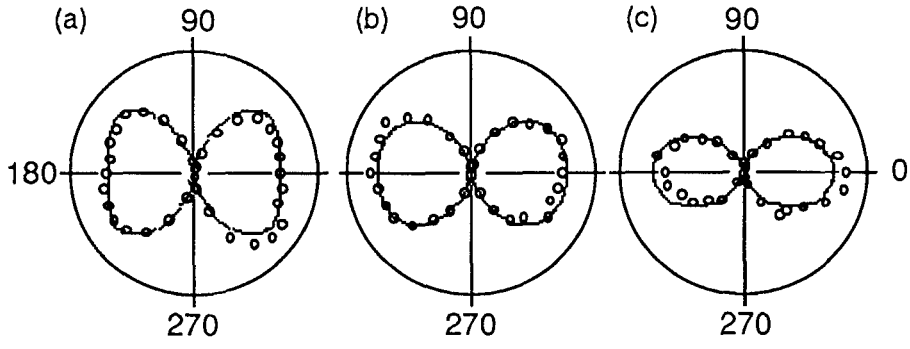

FIGURE 8 SH intensity profiles from vacuum deposited PVDF films under the following conditions (substrate temperature, poling field); (a) 80°C, 10 MV/m, (b) 80°C, 16 MV/m and (c) -130°C, 16 MV/m. Solid curves are theoretical fittings, which give values of χ_{zzz}/χ_{zxx}, (a) 1.63, (b) 2.05 and (c) 3.01.

the conditions described in the caption. The radial length represents the SH intensity observed with the incident angle of 0° as a function of rotation angle of the parallel polarizers, where 0° corresponds to the applied field direction. The solid curves are simulated ones using the projection model, leading to the χ_{zzz}/χ_{zxx} values, (a) 1.63, (b) 2.05 and (c) 3.01. These values, namely the degree of dipole alignment, depend on the poling field and the substrate temperature during deposition. We confirmed that the lower substrate temperature gives a higher degree of dipole orientation and that the field-assist deposition produces much stabler poled structures than the separate process of deposition and post-poling. This experiment suggests the possible application of this surface SHG technique to monitor the deposition process.

π-Conjugated Polymer

It is known that rigidly linear π-conjugated polymers such as poly(pyridine-2,5-diyl), form thin films on various substrates when they are deposited under vacuum[12]. We found that some of the π-conjugated polymer films on a glass substrate show SHG with in-plane anisotropy, although no dichroism was observed in its UV-visible spectrum[13]. This SH activity is attributed to the interfacial structure between the film and the glass substrate. Figure 9 shows the SH intensity profiles observed with 45° incident light in the transmitted direction in poly(2,2'-bipyridine-5,5'-diyl) (PBPy) on a glass substrate. The simulated solid curves

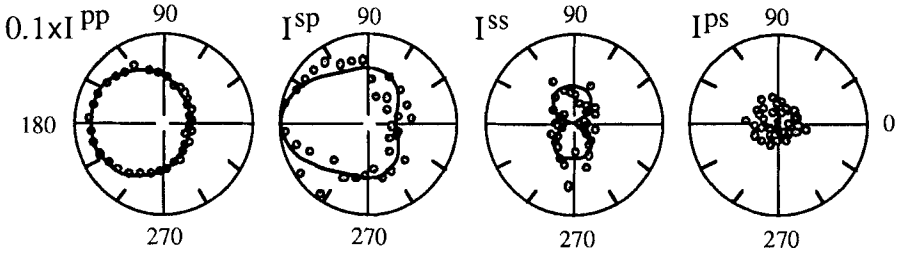

FIGURE 9 SHG intensity profiles from vacuum deposited PBPy on a glass substrate. Solid curves are theoretical fittings.

are based on the strict expressions using C_s symmetry, which is formed by the coordination of the unit of PBPy to acidic-H of the glass substrate[13]. Thus, very sensitive selective observation of the interfacial structure is possible using the surface SHG technique.

Hemicyanine

Figure 10 shows examples of the SH intensity as a function of polarizer rotation angle for a mixture of hemicyanine and arachidic acid[6]. The samples are monomolecular films (a) on the water surface (molecular area of 25 $Å^2$) and (b) on a glass substrate. The circles and squares are data for parallel and crossed polarizers and can be simulated by eqs.(13) and (14), respectively, as shown by solid curves in Fig.10. It should be noted that the agreement between the experiment and calculation is reasonably good. Because of the fitting procedure, by taking account of Fresnel conditions such as reflection loss and multiple reflection inside the film, instead of using only s- and p-polarized SH intensities, we can deduce reliable quantitative values of nonlinear optical and structural quantities. We found that the

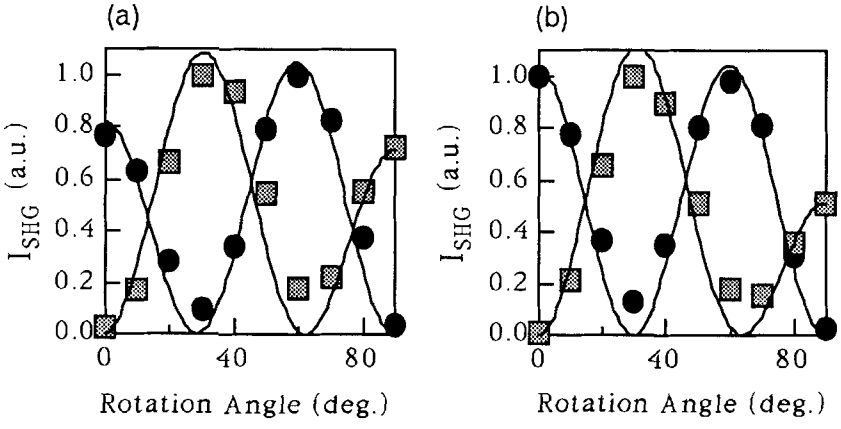

FIGURE 10 SH intensities as a function of polarizer rotation angle for monolayer films of a mixture of hemicyanine and arachidic acid (a) on the water surface and (b) on a glass substrate. The circles and squares are data for parallel and crossed polarizers. The solid curves are best theoretical fittings.

average tilt angle Θ changes from 61° to 51° by the vertical deposition process. Thus, the surface SHG technique can be applied to any circumstances, such as on the water surface and on a substrate.

Merocyanine

While hemicyanine LB films show no SHG for the normal incidence of fundamental light because of $C_{\infty v}$ symmetry with its symmetry axis along the film surface normal, merocyanine LB films show strong SHG in the same optical geometry. This observation suggests the existence of a polar structure in the merocyanine LB film plane. This anisotropic structure is caused by the flow alignment of J-aggregates during deposition.

Figure 11 shows the SH intensity profiles observed with 45° incident light in the transmitted direction[14]. Simulation was made using C_{2v} symmetry as illustrated by solid curves. We also confirmed that there is no anisotropy in the SH intensity profile from merocyanine J-aggregates on the water surface. Therefore, the in-plane anisotropy is produced by flow due to deposition It is noticed that the cut between the leaves is not so sharp as compared with those in Fig.8. This is due to the orientational distribution of the J-aggregates or their domains which are larger than the wavelength used. It was found that the average orientation of these polar axes is preserved over some mm range[14]. If we focus the beam, we can measure the spatial

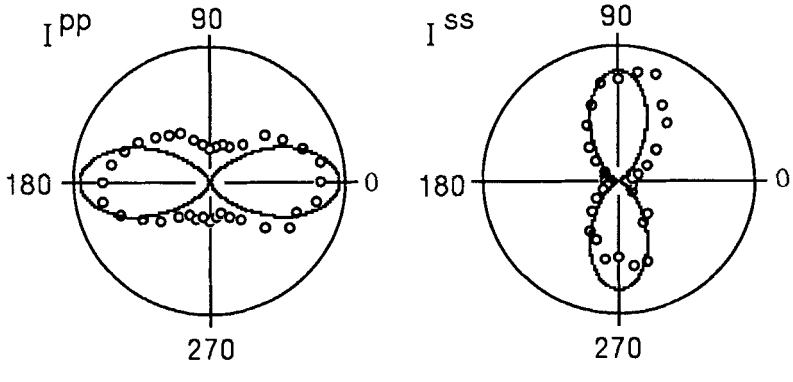

FIGURE 11 SH intensity profiles from a merocyanine LB film. Solid curves are theoretical fittings.

distribution of the SH active structure with the spatial resolution of micrometer range.

In order to clarify the structure of the J-aggregates or their domain structure, we observed the transmitted SH light as rotating the substrate with the films on both sides around the axis parallel to the surface. The results are shown in Fig.12. We can clearly observe interference pattern for I^{pp}, while not for I^{ss}. This fact indicates that the interference pattern in I^{pp} originates from the optical field perpendicular to the substrate, since the inversion symmetry is uniformly broken by the interfaces of both surfaces. On the contrary, in-plane components of the SH field do not interfere or the interference patterns are smeared out. We can interprete that the J-aggregates and/or their domains align along an average direction but with random senses, in other words no macroscopic polarization. The details will be reported elsewhere. Thus, the surface SHG technique supplies information which cannot be obtained by other techniques such as polarized absorption spectra.

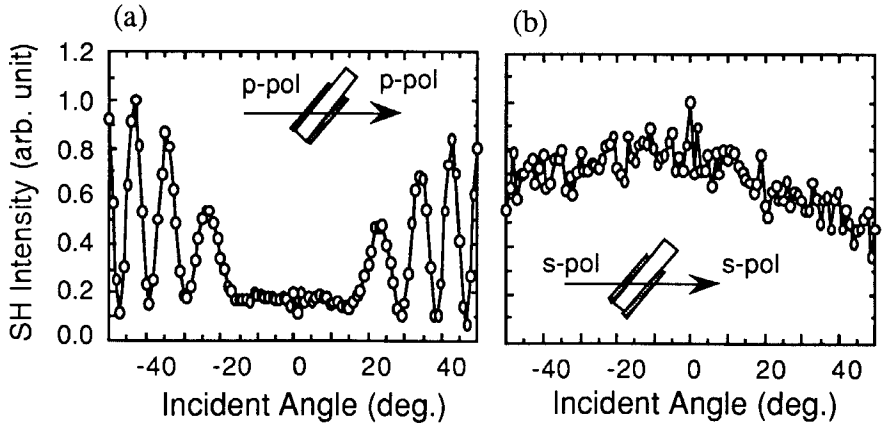

FIGURE 12 Incident angle dependence of the transmitted SH intensities, (a) I^{pp} and (b) I^{ss}, from monomolecular films of merocyanine on both sides of a glass substrate.

Spiropyrane

Spiropyrane is one of the most famous photochromic molecules and has been studied by means of optical methods. In the

monomolecular film of photomerocyanine photoisomerized from spiropyran (SP1822), we recently found that J-aggregates dissociate to monomers and a new J-aggregate band starts to grow. During the process, the SH intensity monotonically decreases with the decrease of the initial J-aggregates irrespective of the increase of the new J-aggregates. Thus, there are two kinds of J-aggregates which have different structures. The SHG measurement can follow this kind of relaxation process. The details will be reported elsewhere.

Dye-Pendant Polymer

Polymer LB films are very attractive because of its chemical and physical stability. However, the study of polymer monolayers is scarce. For the optical measurement, ellipsometry[15,16] and surface light scattering[17] have been applied to the polymer film on the water surface. We applied the surface SHG measurement to a film of polymer with pendant chromophore (PMMA partially substituted by disperse red dye). Based on the same kind of measurement as that in hemicyanine, we determined Θ and χ_{ijk} as a function of molecular area[18,19].

In order to determine molecular susceptibility, $\beta\xi\xi\xi$, we estimated effective local field factor, $L=L_z(2\omega)L_z(\omega)^2$. Using the first equation of eq.(5), L can be determined as shown in Fig.13(a),

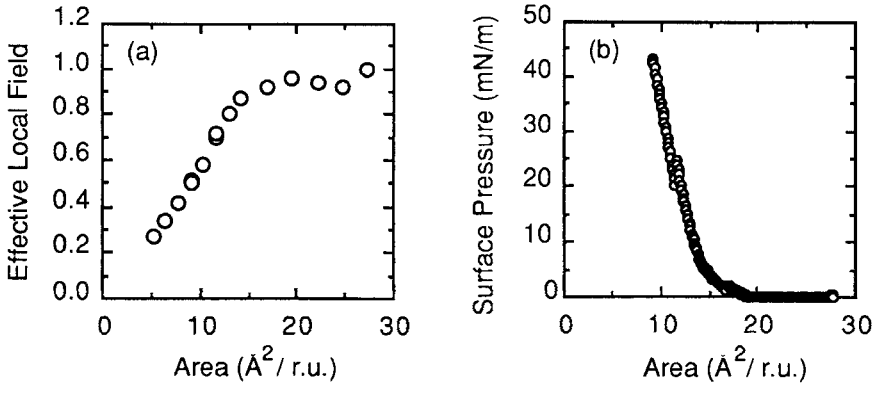

FIGURE 13 (a) Effective local field factor and (b) surface pressure as a function of molecular area.

where L at the widest molecular area is taken as unity[19]. Since L increases and saturates above 20 $Å^2$, it is safe to consider that L is approximately equal to one. The obtained $\beta_{\xi\xi\xi}$ is 1.2×10^{-28} esu, which is a reasonable value for this kind of molecules.

SUMMARY

We summarized the methods of determination of nonlinear optical quantities and of structural analysis based on surface SHG. After explaining the qualitative analysis (projection model), we pointed out matters which demand particular attention and assess the difference between the projection model and the quantitative analysis. We reviewed our experimental works on organic thin films; vacuum evaporated films and Langmuir-Blodgett films. Based on the experimental results, we showed the advantages of this method; (1) high sensitivity, (2) *in situ* observation and (3) spatial resolution.

REFERENCES

1. Y. R. Shen, Nature, **337**, 519 (1989).
2. B. Dick, A. Gierulski, G. Marowsky and G. A. Reider, Appl. Phys., **B38**, 107 (1985).
3. N. Bloembergen and P. S. Pershan, Phys. Rev., **138**, 606 (1962).
4. Y. R. Shen, The Principles of Nonlinear Optics (John Wiley & Sons, Inc., New York, 1988).
5. W. Chen, Ph.D Dissertation (University of California, Berkeley, 1990).
6. K. Kajikawa, H. Takezoe and A. Fukuda, Jpn. J. Appl. Phys., **30**, 1050 (1991).
7. K. Kajikawa, K. Kigata, H. Takezoe and A. Fukuda, Mol. Cryst. Liq. Cryst., **182A**, 91 (1990).
8. H. Nagamori, K. Kajikawa, H. Takezoe, A. Fukuda, S. Ukishima, M. Iijima, Y. Takahashi and E. Fukada, Jpn. J. Appl. Phys., **31**, L553 (1992).
9. Y. Takahashi, M. Iijima and E. Fukada, Jpn. J. Appl. Phys., **28**, L2245 (1989).

10. K. Kajikawa, H. Nagamori, H. Takezoe, A. Fukuda, S. Ukishima, Y. Takahashi, M. Iijima and E. Fukada, Jpn. J. Appl. Phys., **31**, L553 (1992).
11. A. Kubono, T. Kitoh, K. Kajikawa, S. Umemoto, H. Takezoe, A. Fukuda and N. Okui, Jpn. J. Appl. Phys., **31**, L1195 (1992).
12. T. Yamamoto, C. Mori, H. Wakayama, Z. -H. Zhou, T. Maruyama, T. Kanbara and R. Ohki, Chem. Lett., 1483 (1991)
13. T. Fukuda, T. Kanbara, T. Yamamoto, T. Fujioka, K. Kajikawa, H. Takezoe and A. Fukuda, Mol. Cryst. Liq. Cryst. Lett., in press.
14. K. Kajikawa, H. Takezoe and A. Fukuda, Jpn. J. Appl. Phys., **30**, L1525 (1991).
15. B. B. Sauer, H. Yu, M. Yazdanian, G. Zografi and M. W. Kim, Macromolecules, **22**, 2332 (1989)
16. N. Nagata and M. Kawaguchi, Macromolecules, **23**, 3957 (1990).
17. M. Kawaguchi, M. Sano, Y. L. Chen, G. Zografi and H. Yu, Macromolecules **19**, 1206 (1986).
18. K. Kajikawa, T. Anzai, H. Takezoe, A. Fukuda, S. Okada, H. Masuda, H. Nakanishi, T. Abe and H. Ito, Chem. Phys. Lett., **192**, 113 (1992).
19. K. Kajikawa, T. Anzai, H. Takezoe, A. Fukuda, S. Okada, H. Masuda, H. Nakanishi, T. Abe and H. Ito, Langmuir, in press.